Control of Lipid Domain Organization by a Biomimetic Contractile Actomyosin Cortex

Sven K. Vogel[1†], Ferdinand Greiss[1,2,3†], Alena Khmelinskaia[1,3] and Petra Schwille[1]

[1]Max-Planck Institute of Biochemistry, Am Klopferspitz 18, D-82152 Martinsried, Germany
[2]Systems Biophysics, Physics Department, Ludwig-Maximilians-Universität München Amalienstr. 54, D-80799 Munich, Germany
[3]Graduate School of Quantitative Biosciences, Ludwig-Maximilans-University, Feodor-Lynen-Str. 25, D-81377 Munich, Germany

[†] Contributed equally

Abstract

The cell membrane is a heterogeneously organized composite with lipid-protein micro-domains. The contractile actin cortex may govern the lateral organization of these domains in the cell membrane, yet the underlying mechanisms are not known. We recently reconstituted minimal actin cortices (MACs) (Vogel et al, 2013b) and here introduced phase-separated lipid membranes to the MACs to investigate effects of rearranging actin filaments on the lateral membrane organization. We found that the total contour length of the phase boundary increased upon the addition of actin filaments and reached a steady state where line tension and lateral crowding are balanced. The line tension allows myosin driven actin filament rearrangements to actively move individual lipid domains, often accompanied by their shape change, fusion or splitting. Our findings illustrate how myosin induced actin cortex remodeling in cells may control dynamic rearrangements of lipids and other molecules inside those domains without directly binding to actin filaments.

Introduction

The spatiotemporal organization of lipids, proteins and other molecules at and within the cell membrane is pivotal for many fundamental cellular processes, such as signal transduction from the extracellular to the intracellular space (Groves & Kuriyan, 2010). Recent findings over the last years suggest that the cell membrane should be considered as a heterogeneous lipid protein layer with coexisting small micro domains and clusters of lipids and proteins that are assumed to dynamically form and reorganize in response to external and internal cues (Engelman, 2005; Simons & Gerl, 2010). Whether and how their spatiotemporal organization is actively regulated and maintained by the cell remains to be revealed. *In vivo and in vitro* studies suggest an important role of the eukaryotic actin cytoskeleton that directly interacts with the cell membrane via membrane-associated proteins (Heinemann et al, 2013; Murase et al, 2004; Sheetz et al, 1980). Actin structures were found to mediate the lateral organization of membrane proteins (Gudheti et al, 2013) and to modulate their diffusive behavior (Heinemann et al, 2013; Honigmann et al, 2014; Murase et al, 2004). Theoretical considerations have proposed a key role of the actin motor myosin for organizing and forming distinct protein and lipid micro-domains in cell membranes (Gowrishankar et al, 2012). However, direct experimental evidence for a control of micro-domains by actomyosin is still lacking.

In eukaryotic cells, the actin cortex is constantly rearranged by the motor protein myosin II and dozens of actin binding proteins. Therefore, reducing the complexity of experimental conditions, e.g. reducing dimensionality or exploiting a minimal biomimetic system, and utilizing microscopic techniques with a high temporal resolution is beneficial for studying these processes. Phase-separated lipid bilayers with controlled lipid compositions are well-established test beds to mimic lipid micro-domains in cell membranes and biological processes, e.g. the lateral organization of proteins that are otherwise difficult to observe *in vivo*. Ternary mixtures of lipids below their characteristic melting temperature (Tm) can phase separate into liquid disordered (L_d) and liquid ordered (L_o) domains. Liu and Fletcher used phase-separated giant unilamellar vesicles (GUVs) as a model system to study the influence of branched actin networks on the miscibility transition temperature (Liu & Fletcher, 2006). They reported that the formation of localized actin networks on PIP_2-containing phase-separated GUVs could act as switch for the orientation of lipid

domain growth sites.

However, the effects of an actin meshwork on individual lipid domains are technically difficult to study, due to the 3-dimensional architecture of the GUVs. We therefore made use of a minimal biomimetic system of planar geometry that we recently developed (Vogel et al, 2013a; Vogel et al, 2013b) and combined the minimal actin cortex (MAC) with supported phase-separated membranes and lipid monolayers. We then visualized and studied the effects of actin filament adhesion and myosin driven rearrangements on the lateral organization of membrane domains with total internal reflection microscopy (TIRFM) and confocal spinning disk microscopy.

Results

Actin filament partitioning on phase-separated membranes

The effects of adhesion and myosin induced contraction of an actin meshwork on the lateral organization of lipid domains was studied by combining phase-separated lipid membranes with our established assay featuring contractile MACs (Vogel, 2016; Vogel et al, 2013a; Vogel et al, 2013b) (Fig. 1A). For the preparation of phase-separated lipid bilayers, a ternary lipid mixture with DOPC, DPPC and Cholesterol in a 1:2:1 molar ratio was used. Similar lipid compositions were described to form L_o and L_d phases in free-standing membranes up to 30 °C (Veatch & Keller, 2003; Veatch & Keller, 2005). The low miscibility transition temperature of the mixture avoids thermal degradation of proteins and allowed us to study the phase transition behavior in the presence of actin filaments. The fluorescent probe DiD (0.03 mol%) was used to label the L_d phases (Garcia-Saez et al, 2007). The density of biotinylated actin filaments was controlled by the concentration of biotinylated lipid DSPE-PEG(2000)-Biotin (see also (Vogel, 2016; Vogel et al, 2013b)). As observed with TIRF microscopy, the membrane separated into micrometer-sized L_o and L_d domains (Fig. 1B-E) and homogenized at ~37 ºC. The observed shift of 7 °C in Tm compared with studies from (Veatch & Keller, 2003) agreed with our expectations considering the interaction of lipid molecules with the mica support (Garcia-Saez et al, 2007).

The adhesion of actin filaments via neutravidin to biotinylated DSPE provided a stable link between the MAC and the lipid bilayer over a wide range of temperatures.

To validate the partitioning preference of all molecular components, the fluorescence signals of labeled neutravidin and actin filaments were acquired after domain formation when cooled below Tm (Fig. 1B-E). We found that both neutravidin and actin filaments partitioned into L_o phases (Fig. 1B and C). We therefore concluded that the biotinylated lipid DSPE partitioned into L_o phases, and that the concentration of Biotin-DSPE controlled the amount of bound actin filaments to the membrane in an easy and reliable manner (see also (Vogel, 2016; Vogel et al, 2013b)).

Actin filament crowding effects in phase-separated minimal actin cortices

We prepared low (0.01 mol % DSPE-PEG2000-Biotin) and medium (0.1 mol % DSPE-PEG2000-Biotin, Fig. 2B) dense MACs to investigate the effect of actin filament density on phase-separated membranes. To this end, the ternary lipid mixture was incubated with non-labeled neutravidin and placed on a temperature-controlled microscope objective. A fluorescence image was acquired as a reference before actin filaments were added (Fig. 2A and B, left column). A homogeneous membrane was produced by heating the microscope objective to 42 °C (above Tm). Actin filaments were added to the membrane above Tm (Fig. 2A and B, middle column) and the sample was subsequently incubated for ~45 min at 42 °C (Fig. 2A). The membrane was completely covered by actin filaments after approximately 30 minutes (Fig. 2A and B, middle column). Finally, the membrane was slowly cooled down to 30 °C without active cooling and the fluorescence signal recorded after complete phase separation (Fig. 2A and B, right column).

While the low density MAC did not show any influence on membrane domain properties, the medium dense MAC caused the formation of smaller domains (Fig. 2B, right column). Both, actin filaments and DSPE-PEG2000-Biotin partitioned into L_o phases (Fig. 2B and D), confirming our initial partition observations (Fig. 1B - E). We conclude that actin filaments act as nucleation sites for domain formation and drive their lateral spatial distribution.

To investigate the relation between line tension and the binding of actin filaments, we exposed the membrane to different temperatures below Tm and added actin filaments to high density MACs containing a lipid mixture with 1.0 mol% biotinylated DSPE (Fig. 2D - F). We expected a constant binding of actin filaments at moderate temperature changes, due to the strong binding affinity of neutravidin and biotin. Indeed, we found that the integrated fluorescence intensity of labeled actin filaments

was independent of the base temperature (Fig. 2F). Hence, the adhesion process of actin filaments to the membrane and hence crowding is apparently constant over the employed temperature range. The line tension γ between L_o and L_d domains is known to be a linear function of temperature with $\gamma \approx \gamma_0(T_C - T)/T_C$ where T_C is the critical temperature (Baumgart et al, 2003; Honerkamp-Smith et al, 2008; Veatch et al, 2008). With the temperature-independent binding, the final contour length L then increases linearly with a constant boundary energy $E = \gamma$ as induced by the actin filaments(Yang et al, 2016).

Fluorescently labeled actin filaments were added to the sample chamber at various base temperatures below Tm and imaged for ~30 min using TIRF microscopy (Fig. 2D). The contour length (L) (Fig. 2C) of membrane domains was extracted (Canny edge detection) and tracked over time (Fig. 2E). After ~1 min of actin filament addition, first domain deformations could be observed (Fig. 2D (upper row)) and the contour length was found to grow until a steady state at ~60 min was reached (Fig. 2E). Furthermore, the final contour length increased as expected with temperature (final contour lengths: L_{Final} = 286.0±42.3 µm and τ = 38.6±7.7 min at 24 °C, L_{Final} = 518.2±3.9 µm and τ = 7.6±0.2 min at 30 °C, L_{Final} = 1104.3±4.2 µm and τ = 5.6±0.1 min at 36 °C).

Actomyosin contraction governs lateral membrane domain organization

Aster shaped actomyosin clusters form *in vivo* and *in vitro* upon myosin's contractile activity (Backouche et al, 2006; Munro et al, 2004; Murrell & Gardel, 2012; Soares e Silva et al, 2011; Vogel et al, 2013b). Synthetic myofilaments contract the MAC in the presence of ATP and, hence rearrange actin filaments that eventually form stable actomyosin clusters (Fig. 3A-C; Video 1). L_d membrane domains were found to deform within minutes upon contraction, and thereby result in various splitting and fusion events of single domains (Fig. 3E; Videos 2-4). L_d domain shape changes, such as inward ingression, were observed, which correlate with the movement of actomyosin clusters against the L_d domain, thereby exerting pushing forces against the phase boundary (Fig. 3E; Videos 3 and 4). Pushing of actomyosin clusters against smaller L_d domains results in their net movement and may lead to splitting and fusion events with other L_d domains (Fig. 3E; Video 4).

In order to mimic free-standing membranes without support-induced friction of the

SLBs but keeping the technical advantages of a planar geometry, we made use of a recently developed lipid monolayer system (Chwastek & Schwille, 2013) with an air-liquid interface (Fig. 3F). Actin filaments were coupled to ternary phase-separated lipid monolayers similar to the situation in the supported lipid bilayer system via biotinylated lipids and the use of neutravidin. Contrary to the situation in the SLB system, actin filaments preferentially bind to the liquid extended (disordered) (L_e) phase where also the neutravidin anchor protein mainly partitioned to (Fig. 3F), likely due to the different lipid mixture we used here (see Material and Methods). In low and medium dense monolayer MACs the liquid condensed (ordered) L_c domains acquire circular shapes and the actin filaments close to the phase boundaries align to their circular shape (Fig. 3F). In the case of low and medium densities we expect that the line tension energy dominates over the actin filament wetting energy at the phase boundary and hence the L_c can assume an unrestricted shape with aligned actin filaments. Similar effects have been observed using bacterial cytoskeleton proteins (Arumugam et al, 2015). Having this system in hands we were now able to confirm that it is indeed active forces exerted by myosin motors on actin filaments that deform the L_c domains in the monolayer system. The addition of myosin filaments in the presence of ATP led to the contraction of the actin layers and to shape deformations and spatial rearrangements of the L_c domains by the contracting actin filaments (Video 5). The shape changes included fusion and stretching of the L_c domains (Video 5). Note that these “active” deformation forces were only exerted in the presence of myosin filaments and ATP. Interestingly, the obtained lipid domain shapes seem to be stabilized after the active contraction period, probably by the remaining actin filaments. Using the monolayer system also tells us that the frictional force caused by a solid support in SLBs does not play a significant role in the observed phenomena.

Discussion

As cells may need to quickly adapt the macro-and microscopic organization of lipid and protein aggregates within the cell membrane due to external or internal cues, we propose that actomyosin driven reorganization of actin filaments may aid to quickly reorganize their lateral distribution. Recent evidence exists that the presence of an actin meshwork influences the lateral diffusion behavior of lipids and proteins in

membranes *in vivo* (Murase et al, 2004) and *in vitro* (Heinemann et al, 2013) and that it impacts the behavior of phase-separated membranes (Honigmann et al, 2014; Liu & Fletcher, 2006). The important role of myosin is further supported by recent theoretical and *in vitro* studies (Gowrishankar et al, 2012; Koster et al, 2016). It is therefore tempting to speculate that cortical actomyosin contractility may be a generic model for eukaryotic organisms not only to control their mechanical stability and shape but also to quickly and actively control the lateral lipid and protein organization at the cell membrane.

In our MACs that were combined with ternary lipid mixtures we found that binding of actin filaments to a homogeneous bilayer at temperatures above Tm induced spatial alignment of L_o domains to actin bound locations upon cooling below Tm (Fig. 2). Eventually, actin filaments serve here as nucleation sites for domain formation and drive their lateral spatial distribution. We further give direct evidence that the dynamic reorganization of actin filaments by myosin motors actively changes the macroscopic organization of membrane domains in our reconstituted phase-separated lipid bilayers and monolayers. We propose that the transition energy between the L_d and L_o phases (Baumgart et al, 2003; Garcia-Saez et al, 2007; Honerkamp-Smith et al, 2008) enabled the lipid anchored actin filaments to exert lateral forces on the phase boundaries leading to a macroscopic motion of lipid domains that eventually resulted in splitting, fusion or deformation of the lipid domains and in their overall increase in number during and after the actomyosin contraction (Fig. 3; Videos 1-4). Our macroscopic observations may be explained with a simple model on a microscopic level. In this model we would first consider a biotinylated lipid being dragged by an actomyosin filament (Fig. 3G). The actomyosin filament would be associated with lipid phases (L_o and L_d) having unequal viscosities. The drag is then counteracted by friction and would lead to domain deformation and rearrangement. Here, the force propagation would be independent of phase boundaries. As a second independent consideration, the biotinylated lipid would need to overcome the transition barrier between phases while being dragged over a boundary (Fig. 3G). Since our contraction experiments primarily showed that the boundaries deformed locally at actomyosin contraction sites and that actomyosin foci formed at the vicinity of phase boundaries (Fig. 3E, Videos 1-5), we consider the $L_o \rightarrow L_d$ transition free energy ΔG as the dictating driving force for phase deformation.

With an estimated line tension of 0.01 pN for a 1:2:1 DOPC:DPPC:Cholesterol

membrane (Baumgart et al, 2003; Garcia-Saez et al, 2007; Kuzmin et al, 2005; Veatch & Keller, 2005) and a free energy of 50 cal/mol for the $L_o \rightarrow L_d$ transition (Almeida, 2011), the energy for one lipid molecule to transition is roughly 30-fold (0.35/0.01) higher than the energy that is needed to elongate the phase boundary by 1 nm. Together with our experimental findings, we can therefore conclude that actively rearranging actin filaments will primarily lead to the deformation of membrane domains. The lateral reorganization of domains readily suggests a plausible mechanism for active lateral rearrangements of membrane components by actomyosin contractions without the need of binding directly to actin filaments.

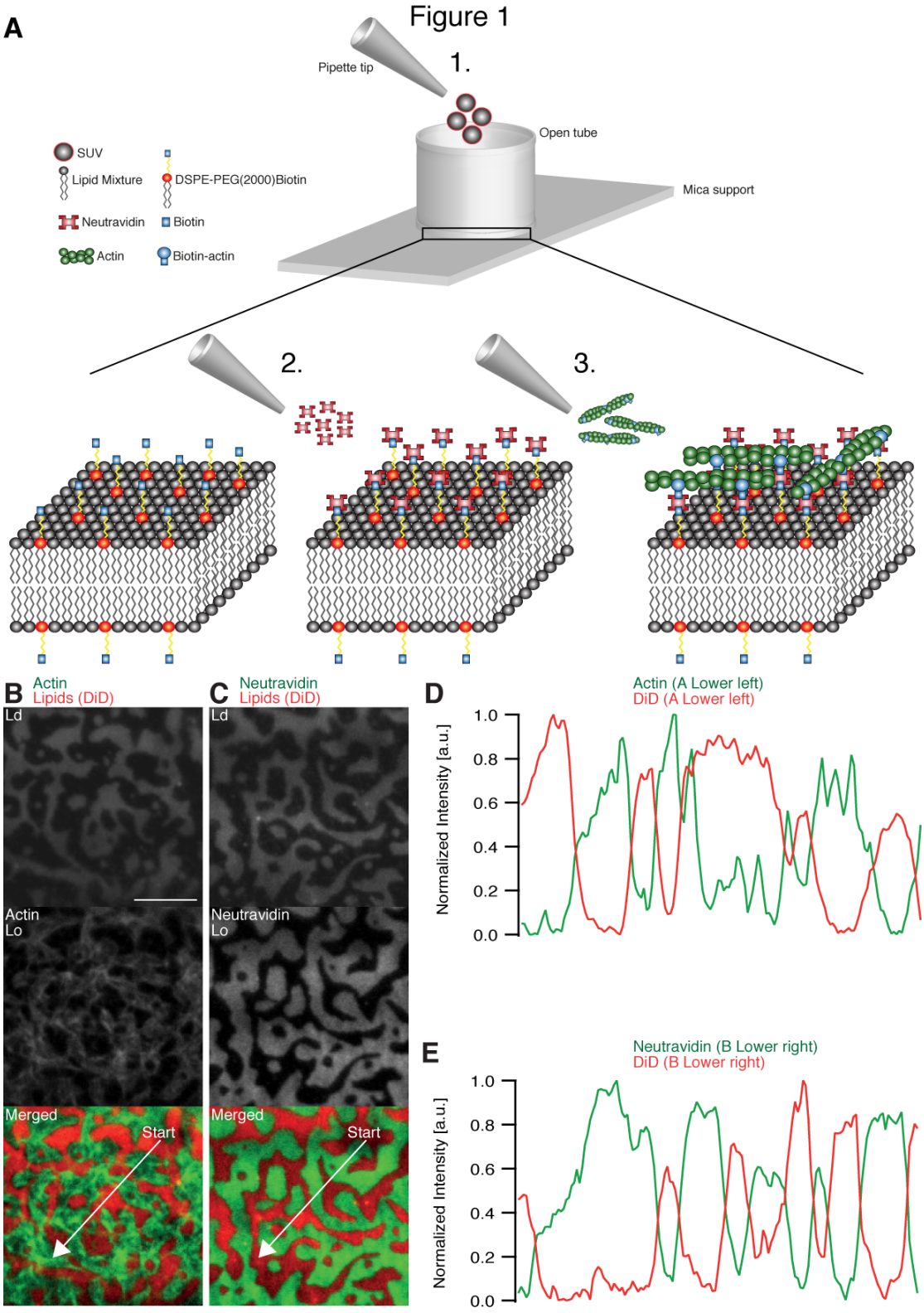

Fig. 1 Minimal actin cortex on a supported phase-separated lipid membrane. (A) Illustration depicting the preparation of the SLB and the coupling of actin filaments to the membrane (Adapted from (Vogel et al, 2013a)). (B) Fluorescence signal indicated the partition of DiD into L_d domains, whereas Alexa-488-phalloidin labeled actin filaments partitioned into the L_o phase. (C) Likewise, Oregon Green labeled Neutravidin partitioned into L_o domains. (D and E) Line profiles of the normalized fluorescence signal of the actin cortex, DiD and Neutravidin as we measured along the superimposed arrows in (B) and (C). Scale bar, 10 µm.

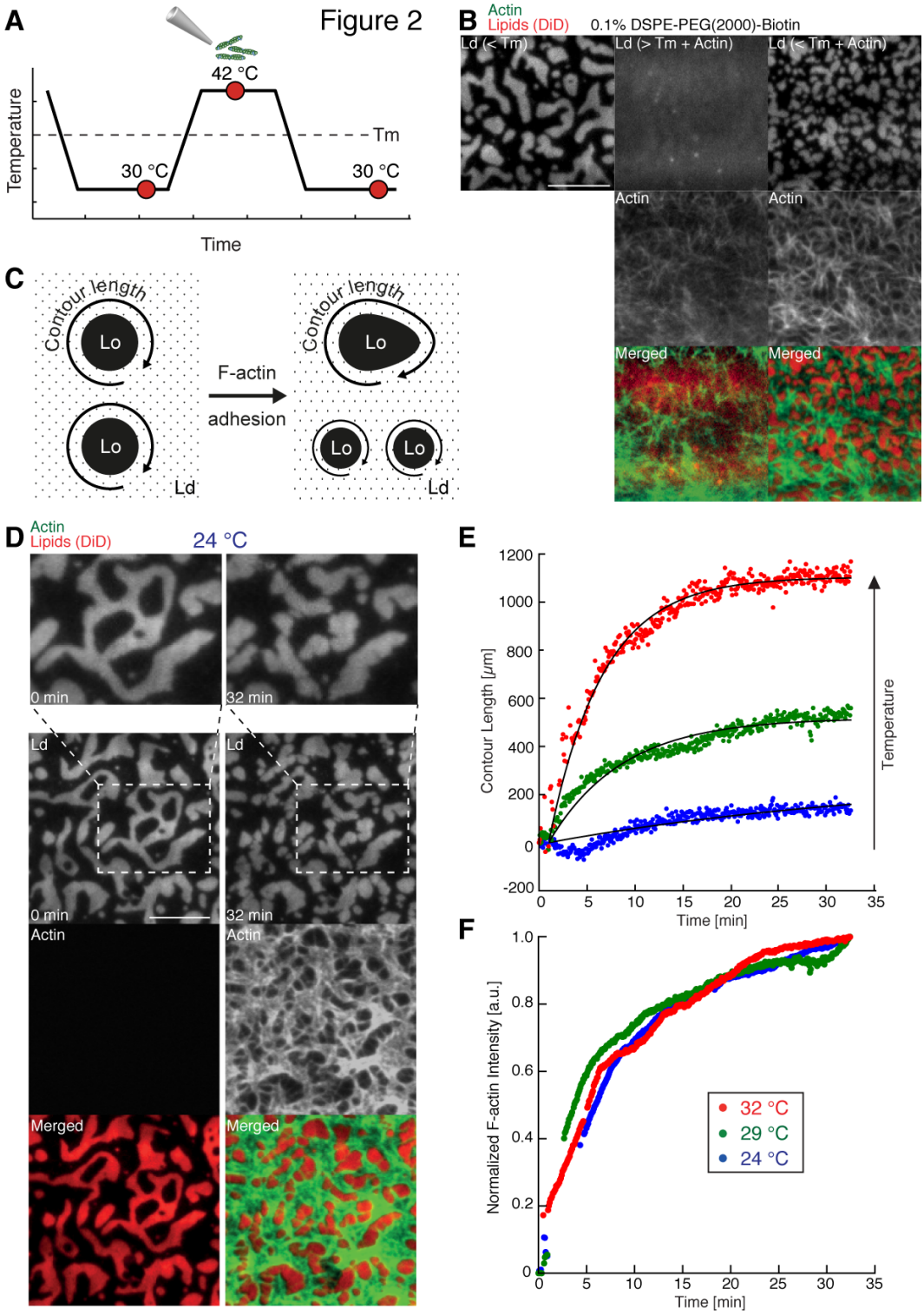

Fig. 2. Increase of the contour length upon actin filament binding to phase-separated membranes at various temperatures. (A) Scheme of the temperature control over time. Circles indicate points in time when fluorescent images were acquired. (B) TIRF images of a medium dense MAC (0.1 mol% DSPE-PEG2000-Biotin) with DiD labeled L_d phases are shown below Tm (30 °C) (left column), above Tm (42 °C) in the presence of bound Alexa-488-phalloidin labeled actin filaments (middle column) and below Tm (30 °C) in the presence of bound actin (right column). The size distribution of L_d domains decreased to smaller areas compared to the reference frame. (C) Sketch of the L_o domain contour lengths before and upon F-actin adhesion. (D) Example of a high density MAC (1 mol% DSPE-PEG2000-Biotin) containing DiD labeled L_d domains and actin filaments is shown before (0 min) and after the addition (32 min) of the actin filaments at 24 ºC. (E) Contour length of L_d domains over time and fits at 24 ºC (blue dots), 29 ºC (green dots) and 32 ºC (red dots). (Note that the observed local dip

in contour length between 2 and 5 min at 24 ºC (blue dots) is due to focal misalignments and subsequent blurring of the acquired fluorescence image after the addition of actin filaments). (F) Normalized fluorescence signal of Alexa-488-phalloidin labeled F-actin over time at 24 ºC (blue dots), 29 ºC (green dots) and 32 ºC (red dots). Scale bars, 10 µm.

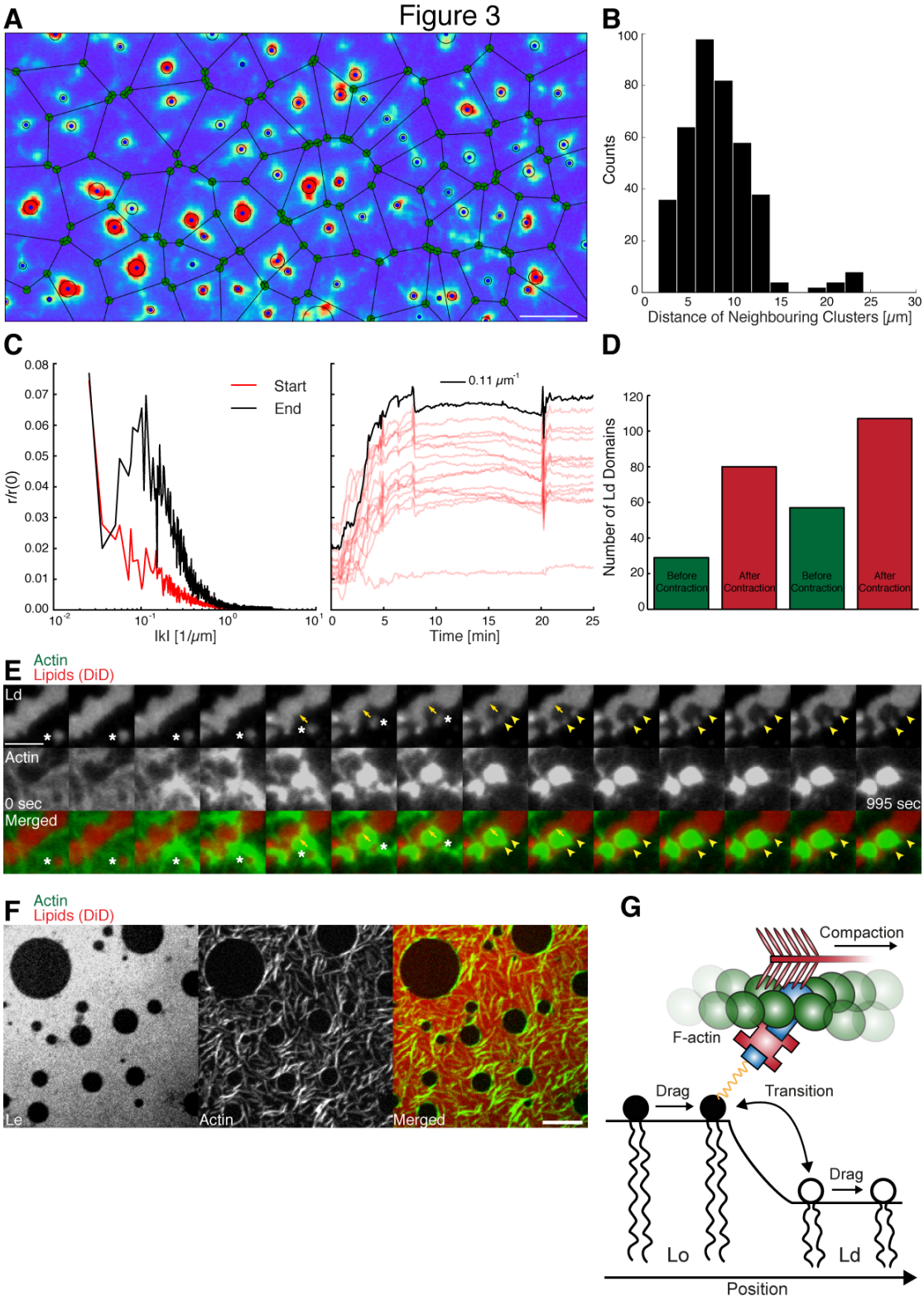

Fig. 3. Actomyosin contraction induces lipid domain movements and shape changes. (A and B) Delaunay triangulation was used to find neighboring actomyosin clusters and their distance distribution. Scale bar, 10 µm. (C) Radially averaged 2-dimensional FFT transformation of the F-actin

channel revealed a maximal frequency after contraction at 0.11 μm^{-1}. The maximal frequency matches the peak in (B). (D) Bar plot of the L_d domain number before (green bars) and after (red bars) actomyosin contraction derived from two independent representative movies. (E) TIRFM time-lapse images of DiD labeled L_d domains and Alexa-488-phalloidin labeled actin filaments in the presence of (non-labeled) myofilaments (0.3 µM) showing the position (movement) of an isolated L_d domain (white asterisks) and its splitting into two separated L_d domains (yellow arrowheads). The movement of the small L_d domain correlates with an inward ingression of the larger L_d domain (yellow arrows). Scale bar, 5 µm. (F) Confocal Spinning Disk images of Alexa-488-phalloidin labeled actin filaments coupled to a DiD labeled lipid monolayer. Scale bar, 10 µm. (G) Scheme of a microscopic model.

Video legends

Video 1: Myosin induced actin rearrangements in a minimal actin cortex (MAC) combined with a supported phase-separated lipid bilayer

MAC with a supported phase-separated membrane containing Alexa-488-phalloidin labeled actin filaments (green) exhibits dynamic rearrangements of actin filaments after the addition of myofilaments in the presence of ATP and eventually forms actomyosin clusters. The phase-separated membrane containing DiD labeled L_d domains (red) is shown in the upper channel. The middle channel shows Alexa-488-phalloidin labeled actin filaments (green) that bind to the L_o domains. The lower channel shows the merge of both channels. TIRFM image sequence was acquired at 5 sec. time intervals and contains 200 frames. The video is displayed at 15 frames per second (fps). Total time: 16.6 min. Scale bar, 10 µm. (Compressed JPG avi; 10.2 MB).

Video 2: Shape changes, rearrangements and fusion events of L_d domains during actomyosin contraction

The phase-separated membrane containing DiD labeled L_d domains (red) is shown in the left channel. The middle channel shows Alexa-488-phalloidin labeled actin filaments that bind to the L_o domains. The right channel shows the merge of both channels. TIRFM image sequence was acquired at 5 sec. time intervals and contains 124 frames. The video is displayed at 15 frames per second (fps). Total time: 10.3 min. Scale bar, 10 µm. (Compressed JPG avi; 0.8 MB).

313 ***Video 3: Splitting, shape changes and deformations of L_d domains during***
314 ***actomyosin contraction***

315 The phase-separated membrane containing DiD labeled L_d domains (red) is shown in
316 the left channel. The middle channel shows Alexa-488-phalloidin labeled actin
317 filaments that bind to the L_o domains. The right channel shows the merge of both
318 channels. TIRFM image sequence was acquired at 5 sec. time intervals and contains
319 200 frames. The video is displayed at 15 frames per second (fps). Total time: 16.6
320 min. Scale bar, 10 µm. (Compressed JPG avi; 0.8 MB).
321

322 ***Video 4: L_d domain movement, splitting and ingression during actomyosin***
323 ***contraction***

324 The phase-separated membrane containing DiD labeled L_d domains (red) is shown in
325 the left channel. The middle channel shows Alexa-488-phalloidin labeled actin
326 filaments that bind to the L_o domains. The right channel shows the merge of both
327 channels. TIRFM image sequence was acquired at 5 sec. time intervals and contains
328 200 frames. The video is displayed at 15 frames per second (fps). Total time: 16.6
329 min. Scale bar, 5 µm. Corresponds to Fig. 3E. (Compressed JPG avi; 0.4 MB).
330

331 ***Video 5: Shape changes and fusion events during actomyosin contraction of L_c***
332 ***domains in a MAC combined with a phase-separated lipid monolayer***

333 Myofilaments in the presence of ATP led to the contraction of the actin layers and to
334 shape changes and fusion events of the L_c domains. The phase-separated lipid
335 monolayer containing the DiD labeled L_e phase (red) is shown in the left channel. The
336 middle channel shows Alexa-488-phalloidin labeled actin filaments that bind to the L_e
337 phase. The right channel shows the merge of both channels. Confocal Spinning Disk
338 image sequence was acquired at 20 sec. time intervals and contains 64 frames. The
339 video is displayed at 15 frames per second (fps). Total time: 21 min. Scale bar, 10
340 µm. (Compressed JPG avi; 1.7 MB).
341
342
343
344

Material and Methods

Actin labeling and polymerization

F-actin preparation was performed as described in (Vogel et al, 2013b). Briefly, a 39.6 µM actin solution (Actin/Actin-Biotin ratio of 5:1) was prepared by mixing rabbit skeletal actin monomers (32 µl, 2 mg/ml, Molecular Probes) with biotinylated rabbit actin monomers (1.6 µl, 10 mg/ml, tebu-bio/Cytoskeleton Inc.). F-buffer (1 mM DTT, 1 mM ATP, 10 mM Tris-HCl (pH 7.4), 2 mM $MgCl_2$ and 50 mM KCl) was added to the mixture in order to start polymerization. Actin polymers were labeled and stabilized with Alexa Fluor 488 Phalloidin according to the manufacturer's protocol (Molecular Probes). Finally, the 2 µM Alexa-488-Phalloidin labeled biotinylated actin filament solution was stored at 4 °C.

MAC (minimal actin cortex) preparation

1,2-dioleoyl-*sn*-glycero-3-phosphorcholine (DOPC), 1,2-dipalmitoyl-*sn*-glycero-3-phosphocholine (DPPC) and cholesterol were added in a molar ratio of 1:2:1 to a final lipid concentration of 5 mg/ml (Avanti Polar Lipids, Inc). The lipid bilayer was further supplemented with 0.03 mol% DiD (Molecular Probes, Eugene, OR) and 0.01, 0.1 or 1 mol% DSPE-PEG(2000)-Biotin (Avanti Polar Lipids, Inc.). The solution was dried under continuous nitrogen flux and then placed under vacuum for 1 h to remove chloroform residuals. The pellet was rehydrated in SLB buffer (150 mM KCl, 25 mM Tris-HCl, pH 7.5) by vigorous vortexing and sonication.

20 µl of clear lipid suspension was then diluted in 130 µl A-buffer (50 mM KCl, 2 mM MgCl2, 1 mM DTT and 10 mM Tris-HCl, pH 7.5) and heated to 55°C. Meanwhile, freshly cleaved mica was fixated with immersion oil (Carl Zeiss, Jena, Germany) on a cover slip (22x22 mm, #1.5, Menzel Gläser, Thermo Fisher) and covered with the center part of a cut 1.5 mL Eppendorf tube. The Eppendorf tube was glued with UV-sensitive glue (Norland Optical Adhesive 63, Cranbury, USA). The chamber was filled with 75 µl of small unilamellar vesicles and incubated at 55 °C for 45 minutes with 1 mM $CaCl_2$. Non-fused vesicles were removed by washing the suspension with 2 ml warmed A-buffer and gentle pipetting. The chamber's temperature was slowly cooled. Next, 2 µl of unlabeled or Oregon-Green labeled neutravidin (1mg/ml, Molecular Probes) diluted in 200 µl A-buffer were added to the

sample and incubated for 10 min. Finally, unbound proteins were removed by gently washing the solution with 2 ml A-buffer.

Phase separation with MAC

The phase-separated membrane was heated with an objective heater (Carl Zeiss, Jena, Germany) to the setpoint of 42 °C and cooled down to 30 °C, both with and without Alexa-488-Phalloidin labeled biotinylated actin filaments. The area distribution of domains at equilibrium (45 min after 30 °C was reached) was then quantitatively compared between the different concentrations of DSPE-PEG(2000)-Biotin (0.1, 0.01 mol%).

Crowding-Effect

The sample was placed on the TIRF microscope objective with attached objective heater and slowly warmed to the setpoint of 42 °C. The lipid bilayer with 1.0 % DSPE-PEG(2000)-Biotin was equilibrated at different temperatures below the melting point (~37 °C for 1:2:1 DOPC:DPPC:Cholesterol). 20 µl of Alexa-488-Phalloidin labeled biotinylated actin filaments were then carefully added to the chamber. Binding of actin filaments to the membrane was recorded by acquiring images in interleaved mode (488 nm and 640 nm respectively) every 2.5 seconds, generating a time-lapse movie with a 5 sec delay between subsequent images.

F-actin network contraction by myofilaments

After the addition of 20 µl Alexa-488-Phallodin labeled biotinylated actin filaments to the supported lipid bilayer at room temperature (~24 °C), the mixture was incubated for approximately 45 min in order to ensure full binding of actin filaments to the membrane. Subsequently, residual actin was removed by gently exchanging the solution with 2 ml A-buffer. Once the properly assembled MAC was verified with TIRF microscopy, a solution of 20 µl myofilaments and 1 µl ATP (0.1 M) were added to start the compaction of actin filaments.

Images were acquired every 2.5 sec in interleaved mode, which eliminated the cross talk between color channels of actin filaments and the phase-separated membrane.

TIRF microscopy

Fluorescent imaging of labeled proteins and membrane was carried out on a custom-

411 built TIRF microscope. The setup was integrated into an Axiovert 200 microscope
412 (Zeiss). The probe was illuminated and imaged through a Plan-Apochromat 100x/NA
413 1.46 oil immersion objective with a 488-nm and 630-nm laser. Images were acquired
414 with an Andor Solis EMCCD camera (electron gain = 300, exposure time = 50 ms,
415 frame interval = 2.5 or 5 sec) in interleaved mode.
416
417 **Data analysis**
418 Image processing, analysis and data visualization was performed with Fiji and the
419 scientific packages for Python. Multichannel beads were used to align double-color
420 image stacks with the Fiji plugin Descriptor-based series registration. The contour
421 length between the lipid domains was extracted by detecting edges (Canny edge
422 detection; (van der Walt et al, 2014)) in single fluorescent images acquired from
423 phase-separated membranes. The contour length over time was fitted to $L =$
424 $L_{Final}\,(1 - \exp(-1/\tau\,(t - t_0)))$ with $t_0 = 1$ min. The actomyosin clusters were
425 detected using the Laplacian of Gaussian method (scikit-image (van der Walt et al,
426 2014)) and assigned to neighbors using the Delaunay triangulation and its method
427 vertex_neighbor_vertices. As supporting method, a 2-dimensional Fast Fourier
428 Transform (FFT) algorithm was deployed in order to analyze the spatial distribution
429 and temporal dynamics of actomyosin cluster formation.
430
431 **MAC assembly on lipid monolayers**

432 The lipids DOPC, C16 sphingomyelin, cholesterol and DSPE-PEG(2000)-biotin
433 (Avanti Polar Lipids, Alabaster, AL) in the molar ratios 42.4:42.4:14.1:1 were mixed,
434 dried under nitrogen flux for 15 min, subsequently put into vacuum for 30 min and
435 dissolved in chloroform (total lipid concentration of 1 mg/ml). The mixture was
436 further diluted to a final lipid concentration of 0.1 mg/ml and labeled by addition of
437 0.1 mol% of ATTO-655DOPE (ATTO-TEC GmbH, Siegen, Germany). The total
438 lipid concentration was confirmed by gravimetry.

439 To form a chamber (see Scheme 1), chamber spacers were cut from a 5mm thick sheet
440 of PTFE by a laser cutter. The spacers were sonicated step by step in acetone,
441 chloroform, isopropanol and ethanol (15 min each). Glass cover slips of 15 mm
442 (Gerhard Menzel GmbH, Braunschweig, Germany) were fixed to the spacer by

443 picodent twinsil® 22 two component glue (picodent®, Wipperfuerth, Germany). The
444 chambers were washed alternately with ethanol and water, air dried and air plasma-
445 cleaned for 10 min in order to make the glass hydrophilic. The surface was then
446 passivated by covering the glass surface with PLL-PEG(2000) (SuSos AG,
447 Dübendorf, Switzerland) 0.5 mg/mL solution in PBS buffer and incubated for
448 minimum half an hour. After throughout wash with water (5 times 200 µl) and
449 reaction buffer (3 times 200 µl), the chambers were ready to use.
450 Lipid monolayers were formed by drop-wise deposition of the lipid mixture on the
451 buffer-air interface (for further details, see also (Chwastek & Schwille, 2013)). A lipid
452 mixture volume corresponding to a lipid surface density of 70 $Å^2$ / molecule was
453 deposited drop-wise on the surface of the buffer solution.

454 The samples were imaged using a Yokogawa scan head CSU10-X1 spinning disk
455 system connected to a Nikon Eclipse Ti inverted microscope (Nikon, Japan) with an
456 Andor Ixon Ultra 512x512 EMCCD camera and a 3i solid state diode laser stack with
457 488 nm, 561 nm and 640 nm laser lines (3il33, Denver, Colorado USA). For
458 simultaneous Alexa-488-phalloidin and DiD excitation, the 488 nm and the 640 nm
459 laser lines and an UPLanSApo 60x/1.20 Water UIS2 objective (Olympus, Japan) were
460 used. The time interval between the recorded images was 20 s.

461 After confirming the formation of a phase-separated lipid monolayer by imaging,
462 100 µl of neutravidin solution (0.01 µg/µl) was added to the sample twice and was
463 incubated for 5 min. Note that all protein solutions or other solutions are applied
464 directly to the liquid subphase by dipping the pipette tip through the monolayer. Next,
465 the subphase was washed 5 times with buffer (100 µl steps) to remove unbound
466 neutravidin. Subsequently, 20 µl of Alexa-488-phalloidin labeled actin filaments
467 (2 µM) was added to the subphase and incubated for at least 60 min, since binding of
468 actin filaments to the interface was assumed to occur relatively slowly. When the
469 binding of the actin filaments was confirmed by imaging, the monolayer was
470 thoroughly washed (7 to 10 steps of 100 µl) with reaction buffer containing 1 µM
471 ATP and 100 µl of myofilaments (0.3 µM) containing 1 µM ATP (enzymatically
472 regenerated see above) was added to the subphase twice. The sample was sealed by a
473 glass cover slide with grease to avoid subphase evaporation, allowing for long sample
474 observation. The lipid monolayer MAC system started to contract after a few minutes

of incubation, resulting in the formation of actomyosin clusters and deformation of the lipid domains.

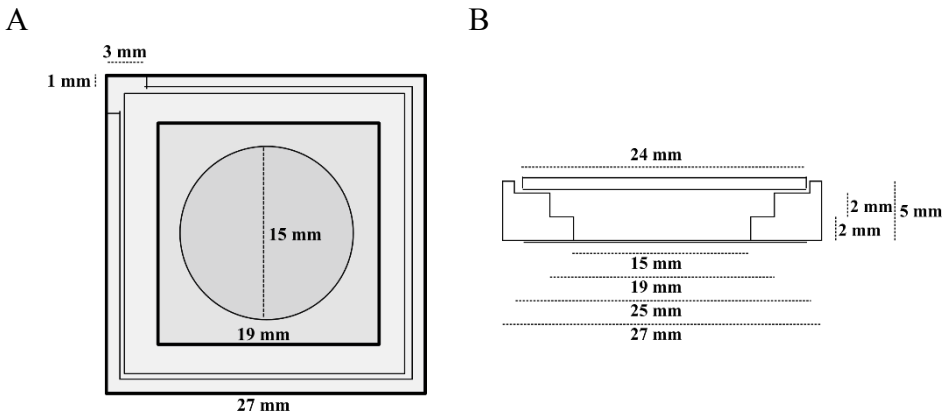

Scheme 1: Top (A) and lateral (B) schematic view of the PTFE chamber (adapted from (Chwastek & Schwille, 2013).

Acknowledgements

We are grateful for the financial support by the Daimler und Benz foundation (Project Grant PSBioc8216), the Gottfried Wilhelm Leibniz-Program of the DFG **(**SCHW716/8-1**),** the support of the Graduate School of Quantitative Biosciences Munich and the MaxSynBio consortium, which is jointly funded by the Federal Ministry of Education and Research of Germany and the Max Planck Society.

References

Almeida PF (2011) A Simple Thermodynamic Model of the Liquid-Ordered State and the Interactions between Phospholipids and Cholesterol. *Biophysical Journal* **100:** 420-429

Arumugam S, Petrov EP, Schwille P (2015) Cytoskeletal pinning controls phase separation in multicomponent lipid membranes. *Biophys J* **108:** 1104-1113

Backouche F, Haviv L, Groswasser D, Bernheim-Groswasser A (2006) Active gels: dynamics of patterning and self-organization. *Phys Biol* **3:** 264-273

Baumgart T, Hess ST, Webb WW (2003) Imaging coexisting fluid domains in biomembrane models coupling curvature and line tension. *Nature* **425:** 821-824

Chwastek G, Schwille P (2013) A monolayer assay tailored to investigate lipid-protein systems. *Chemphyschem* **14:** 1877-1881

Engelman DM (2005) Membranes are more mosaic than fluid. *Nature* **438:** 578-580

Garcia-Saez AJ, Chiantia S, Schwille P (2007) Effect of line tension on the lateral organization of lipid membranes. *The Journal of biological chemistry* **282:** 33537-33544

Gowrishankar K, Ghosh S, Saha S, C R, Mayor S, Rao M (2012) Active remodeling of cortical actin regulates spatiotemporal organization of cell surface molecules. *Cell* **149:** 1353-1367

Groves JT, Kuriyan J (2010) Molecular mechanisms in signal transduction at the membrane. *Nat Struct Mol Biol* **17:** 659-665

Gudheti MV, Curthoys NM, Gould TJ, Kim D, Gunewardene MS, Gabor KA, Gosse JA, Kim CH, Zimmerberg J, Hess ST (2013) Actin mediates the nanoscale membrane organization of the clustered membrane protein influenza hemagglutinin. *Biophys J* **104:** 2182-2192

Heinemann F, Vogel SK, Schwille P (2013) Lateral membrane diffusion modulated by a minimal actin cortex. *Biophys J* **104:** 1465-1475

Honerkamp-Smith AR, Cicuta P, Collins MD, Veatch SL, den Nijs M, Schick M, Keller SL (2008) Line tensions, correlation lengths, and critical exponents in lipid membranes near critical points. *Biophys J* **95:** 236-246

Honigmann A, Sadeghi S, Keller J, Hell SW, Eggeling C, Vink R (2014) A lipid bound actin meshwork organizes liquid phase separation in model membranes. *Elife* **3:** e01671

Koster DV, Husain K, Iljazi E, Bhat A, Bieling P, Mullins RD, Rao M, Mayor S (2016) Actomyosin dynamics drive local membrane component organization in an in vitro active composite layer. *Proc Natl Acad Sci U S A*

Kuzmin PI, Akimov SA, Chizmadzhev YA, Zimmerberg J, Cohen FS (2005) Line tension and interaction energies of membrane rafts calculated from lipid splay and tilt. *Biophysical Journal* **88:** 1120-1133

Liu AP, Fletcher DA (2006) Actin polymerization serves as a membrane domain switch in model lipid bilayers. *Biophys J* **91:** 4064-4070

Munro E, Nance J, Priess JR (2004) Cortical flows powered by asymmetrical contraction transport PAR proteins to establish and maintain anterior-posterior polarity in the early C. elegans embryo. *Developmental cell* **7:** 413-424

Murase K, Fujiwara T, Umemura Y, Suzuki K, Iino R, Yamashita H, Saito M, Murakoshi H, Ritchie K, Kusumi A (2004) Ultrafine membrane compartments for molecular diffusion as revealed by single molecule techniques. *Biophysical journal* **86:** 4075-4093

Murrell MP, Gardel ML (2012) F-actin buckling coordinates contractility and severing in a biomimetic actomyosin cortex. *Proc Natl Acad Sci U S A* **109:** 20820-20825

Sheetz MP, Schindler M, Koppel DE (1980) Lateral mobility of integral membrane proteins is increased in spherocytic erythrocytes.

Simons K, Gerl MJ (2010) Revitalizing membrane rafts: new tools and insights. *Nature Reviews Molecular Cell Biology* **11:** 688-699

Soares e Silva M, Depken M, Stuhrmann B, Korsten M, MacKintosh FC, Koenderink GH (2011) Active multistage coarsening of actin networks driven by myosin motors. *Proc Natl Acad Sci U S A* **108:** 9408-9413

van der Walt S, Schonberger JL, Nunez-Iglesias J, Boulogne F, Warner JD, Yager N, Gouillart E, Yu T, scikit-image c (2014) scikit-image: image processing in Python. *PeerJ* **2:** e453

Veatch SL, Cicuta P, Sengupta P, Honerkamp-Smith A, Holowka D, Baird B (2008) Critical fluctuations in plasma membrane vesicles. *Acs Chem Biol* **3:** 287-293

Veatch SL, Keller SL (2003) Separation of liquid phases in giant vesicles of ternary mixtures of phospholipids and cholesterol. *Biophys J* **85:** 3074-3083

Veatch SL, Keller SL (2005) Miscibility phase diagrams of giant vesicles containing sphingomyelin. *Phys Rev Lett* **94:** 148101

Vogel SK (2016) Reconstitution of a Minimal Actin Cortex by Coupling Actin Filaments to Reconstituted Membranes. *Methods Mol Biol* **1365:** 213-223

Vogel SK, Heinemann F, Chwastek G, Schwille P (2013a) The design of MACs (minimal actin cortices). *Cytoskeleton (Hoboken)* **70:** 706-717

Vogel SK, Petrasek Z, Heinemann F, Schwille P (2013b) Myosin Motors Fragment and Compact Membrane-Bound Actin Filaments. *eLife* **2013;2:e00116**

Yang ST, Kiessling V, Tamm LK (2016) Line tension at lipid phase boundaries as driving force for HIV fusion peptide-mediated fusion. *Nature communications* **7**